OBESITY

Orthopedia regulates melanocortin 4 receptor transcription and energy homeostasis

Baijie Xu[1]†, Katherine Lawler[2]†, Steven C. Wyler[1]†, Li Li[1], Swati[1], Julia M. Keogh[2], Xiameng Chen[1], Rong Wan[1], Amanda G. Almeida[1], Susan Kirsch[3], Kathleen G. Mountjoy[4], Joel K. Elmquist[1], I. Sadaf Farooqi[2]*, Chen Liu[1,5,6]*

Disruption of hypothalamic melanocortin 4 receptors (MC4Rs) causes obesity in mice and humans. Here, we investigated the transcriptional regulation of *MC4R* in the hypothalamus. In mice, we show that the homeodomain transcription factor Orthopedia (OTP) is enriched in MC4R neurons in the paraventricular nucleus (PVN) of the hypothalamus and directly regulates *Mc4r* transcription. Deletion of *Otp* in PVN neurons during development or adulthood reduced *Mc4r* expression, causing increased food intake and obesity. In humans, four of the five carriers of rare predicted functional *OTP* variants in UK Biobank had obesity. To explore a causal role for human *OTP* variants, we generated mice with a loss-of-function *OTP* mutation identified in a child with severe obesity. Heterozygous knock-in mice exhibited hyperphagia and obesity, reversed by treatment with an MC4R agonist. Our findings demonstrate that OTP regulates mammalian energy homeostasis and enable the diagnosis and treatment of individuals with obesity due to *OTP* deficiency.

INTRODUCTION

Neural circuits in the hypothalamus regulate energy homeostasis in mammalian species. The melanocortin pathway consists of neurons in the arcuate nucleus (AN) of the hypothalamus, which either express the anorectic peptide pro-opiomelanocortin (POMC) or the orexigenic peptide Agouti-related peptide (AGRP) (*1*). Both sets of neurons project to the paraventricular nucleus (PVN), where they synapse with neurons expressing the melanocortin 4 receptor (MC4R) (*1*). In the fed state, activation of MC4R signaling by POMC-derived melanocortin peptides leads to suppression of food intake, whereas, in the fasted state, AGRP antagonizes MC4R to increase food intake.

Genetic studies have shown that the melanocortin pathway is pivotal to regulating human food intake and body weight given that loss-of-function (LOF) mutations in *POMC* (*2*), the enzyme that processes POMC [*proprotein convertase subtilisin/kexin type 1* (*PCSK1*)] (*3*), and *MC4R* (*4*) lead to severe childhood-onset obesity. Conversely, gain-of-function mutations that retain MC4Rs at the cell surface are associated with protection from obesity (*5*). These findings demonstrate that quantitative variation in MC4R signaling is important for regulating human energy balance.

Little is known about how *MC4R* expression is regulated in the adult brain. Although MC4Rs are expressed in several brain regions, their expression in the hypothalamus is critical to the regulation of food intake and body weight. For example, deletion of *Mc4r* in PVN neurons causes hyperphagic obesity in mice (*6*), whereas restoring *Mc4r* expression in these neurons is sufficient to normalize hyperphagia in severely obese *Mc4r*-null mice (*7*). Here, we set out to identify regulators of *Mc4r* transcription in the adult hypothalamus. We demonstrate that the homeodomain transcription factor (TF) *Orthopedia* (*Otp*) regulates *Mc4r* transcription in PVN neurons and that a LOF mutation in *OTP* causes obesity in humans, which can be treated with a licensed MC4R agonist.

RESULTS

Identification of transcriptional regulators of *Mc4r* in adult hypothalamic neurons

To identify transcriptional regulators of *Mc4r* in the hypothalamus, we crossed *Mc4r-Cre* mice (*8*) with *Cre* reporter mice (*R26R^{LSL-tdTomato}*, *Ai14*) (*9*) to generate double transgenic mice (*Mc4r-Cre; Ai14*), in which *Mc4r-Cre*–expressing neurons were labeled by the expression of a *Cre*-dependent tdTomato reporter. In situ hybridization (RNAscope) analyses revealed that most tdTomato-positive neurons in the hypothalamus expressed *Mc4r* mRNA (93.0 ± 0.76%; fig. S1, A and B). We purified these neurons by fluorescence-activated cell sorting (FACS) and profiled their transcriptome using bulk RNA sequencing (RNA-seq; Fig. 1A), which revealed an enrichment of 2038 genes [$\log_2$ fold change ($\log_2$FC) > 1 and false discovery rate (FDR) < 0.05] in tdTomato-positive neurons compared with tdTomato-negative cells (Fig. 1A). As expected, transcripts for *Mc4r* were highly abundant in these neurons (119-fold versus tdTomato-negative cells).

We identified 17 TFs that showed significant enrichment ($\log_2$FC > 5 and FDR < 0.05) in tdTomato-positive neurons (Fig. 1B). Seven TFs were conserved between humans and mice (fig. S2A), whereas others were mouse-specific genes [for example, the zinc finger proteins (ZFPs)]. We examined the expression of four TFs (*Dlx5*, *Foxp2*, *Onecut2*, and *Otp*) that are enriched in human hypothalamic neurons (*10*) and demonstrated overlapping expression patterns with *MC4R* (fig. S2B). In the hypothalamus, *Mc4r* expression was mainly confined to subsets of neurons in the anteroventral periventricular (AVPV), paraventricular, anterior hypothalamic (AHN), dorsal medial (DMH), and ventral medial (VMH) nuclei of the hypothalamus

[1]Hypothalamic Research Center, Department of Internal Medicine, UT Southwestern Medical Center, Dallas TX, 75390, USA. [2]University of Cambridge Metabolic Research Laboratories and NIHR Cambridge Biomedical Research Centre, Institute of Metabolic Science, Addenbrooke's Hospital, Cambridge CB2 0QQ, UK. [3]Department of Endocrinology, Hospital for Sick Children, 555 University Avenue, Toronto, ON M5G1X8, Canada. [4]Department of Molecular Medicine and Pathology and Center for Brain Research, University of Auckland, Private Bag 92019, Auckland 1142, New Zealand. [5]Department of Neuroscience, UT Southwestern Medical Center, Dallas, TX 75390, USA. [6]Peter O'Donnell Jr. Brain Institute, UT Southwestern Medical Center, Dallas, TX 75390, USA.
*Corresponding author. Email: Chen.Liu@UTSouthwestern.edu (C.L.); isf20@cam.ac.uk (I.S.F)
†These authors contributed equally to this work.

Fig. 1. Identification of *Otp* as a regulator of *Mc4r* transcription in the PVN of the hypothalamus. (A) Schematic of the purification and transcriptomic analyses of hypothalamic *Mc4r-Cre* neurons. FACS was used to isolate tdTomato-positive *Mc4r-Cre* neurons, and their transcriptome was profiled using bulk RNA-seq. A total of 2038 genes were enriched (log$_2$FC > 1) in tdTomato-positive neurons compared with tdTomato-negative cells. **(B)** Heatmap showing the expression of 17 TFs highly enriched (log$_2$FC > 5) in *Mc4r-Cre* neurons. Color scale indicates relative expression: Darker indicates higher expression. **(C)** Expression of mRNAs for *Dlx5*, *Foxp2*, *Onecut2*, and protein for Otp in tdTomato-positive *Mc4r-Cre* neurons in the AVPV, paraventricular, AHN, DMH, and VMH nuclei of the hypothalamus. Scale bar, 50 μm. **(D)** Summary of the expression patterns of *Dlx5*, *Foxp2*, and *Onecut2* mRNAs and Otp protein in neurons in the AVPV, PVN, AHN, DMH, and VMH regions. Expression is "+++" for highly expressed and "−" for no expression. **(E)** Immunofluorescence of Otp protein (white) in *Mc4r-Cre* neurons (red) in the AVPV, PVN, DMH, and VMH regions. Scale bar, 20 μm. **(F)** Quantification of the percentage of *Mc4r-Cre* neurons expressing Otp protein in the AVPV, PVN, AHN, DMH, and VMH regions (*n* = 4 mice). Data are presented as means ± SEM.
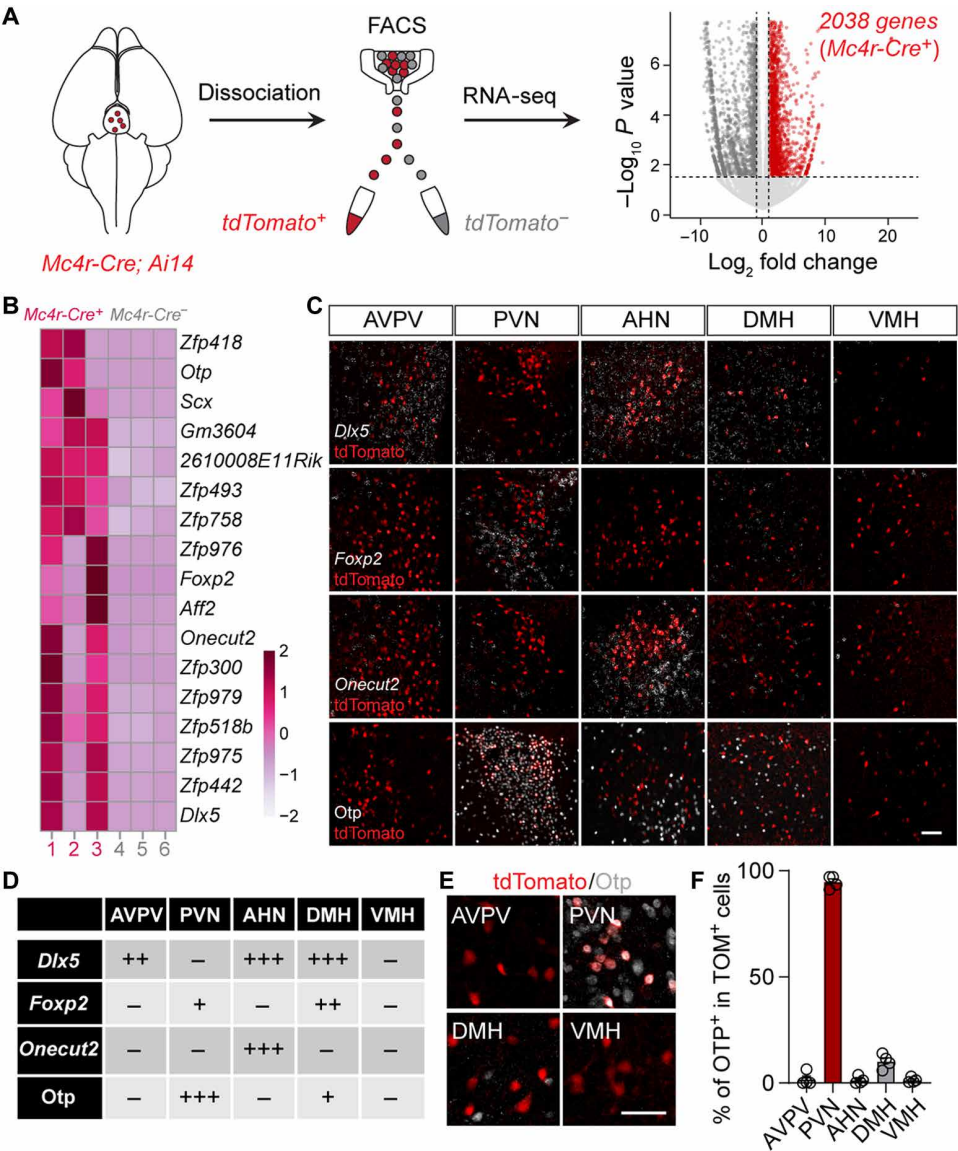
(fig. S2C) (*11*). RNAscope experiments in *Mc4r-Cre; Ai14* mice revealed that the four TFs were selectively expressed by specific subsets of *Mc4r-Cre* neurons: *Mc4r-Cre* neurons in the AVPV, AHN, and DMH regions expressed *Dlx5*, whereas *Onecut2* was only found in *Mc4r-Cre* neurons in the AHN region (Fig. 1, C and D). These findings suggest that the regulation of *Mc4r* transcription in the adult hypothalamus is region-specific and involves distinct transcriptional programs.

Among the TFs that we examined, *Foxp2* and *Otp* were present in the PVN. Given that *Foxp2* is found only in a subset of PVN *Mc4r-Cre* neurons, whereas all expressed *Otp* (Fig. 1, E and F), we hypothesized that *Otp* is a critical regulator of *Mc4r* transcription in the PVN.

Otp interacts with cis-regulatory sequences to modulate *Mc4r* promoter activity

We previously characterized a promoter region of the mouse *Mc4r* gene that comprises the 5′ untranslated region (5′UTR) and 1-kb

upstream sequences capable of driving tissue-specific expression in transgenic mice (Fig. 2A) (*12*). In *Neuro2A* cells lacking endogenous *Mc4r* (*13*), *Otp* dose-dependently increased the expression of a luciferase reporter driven by the same promoter sequence (Fig. 2B). To regulate transcription, Otp likely operates near regions with accessible chromatin. To pinpoint such loci, we conducted an ATAC-seq (assay for transposase-accessible chromatin with sequencing) experiment in the PVNs of 12-week-old mice. For *Mc4r*, a single ATAC peak [540 base pairs (bp)] was detected in the promoter region, spanning the boundary between the 5′UTR and upstream sequences (Fig. 2C). Further analyses revealed that the majority of reads were enriched in two distinct peak subdomains, designated as P1 (142 bp) and P2 (211 bp), respectively (Fig. 2C). To determine whether Otp can directly bind to the *Mc4r* promoter, we performed a CUT&RUN (cleavage under targets and release using nuclease) assay in the adult PVN. Using an Otp antibody, we identified a specific protein-DNA interaction in the promoter region that was absent in the control (anti–immunoglobulin G; Fig. 2D). Notably, the

Fig. 2. Otp regulates *Mc4r* promoter activity in cells. (**A**) Schematic of the luciferase reporter driven by the mouse *Mc4r* promoter consisting of the 5′UTR and 1-kb upstream genomic sequences. (**B**) Fold change in luciferase activity in *Neuro2A* cells transfected with plasmids encoding cDNAs for *Otp*. One-way ANOVA with Dunnett's post hoc test, $F_{2,21}= 21.51$, $P < 0.001$. Results were replicated in three independent experiments. (**C**) Genome browser track of ATAC-seq–normalized reads at the mouse *Mc4r* promoter. The peak (pink line) consists of two subdomains: P1 (orange line) and P2 (blue line). *Y* axis, normalized accessibility (scale, 0 to 0.88). (**D**) Genome browser track of Otp CUT&RUN–normalized reads at the mouse *Mc4r* promoter. Green line, the identified protein-DNA interaction. *Y* axis, normalized coverage track (scale, 0 to 0.15). IgG, immunoglobulin G. (**E**) Fold change in luciferase activity with the ΔP1 promoter; unpaired *t* test. Results were replicated in three independent experiments. (**F**) Fold change in luciferase activity with the ΔP2 promoter; unpaired *t* test. Results were replicated in three independent experiments. Data are presented as means ± SEM. ***$P < 0.001$.
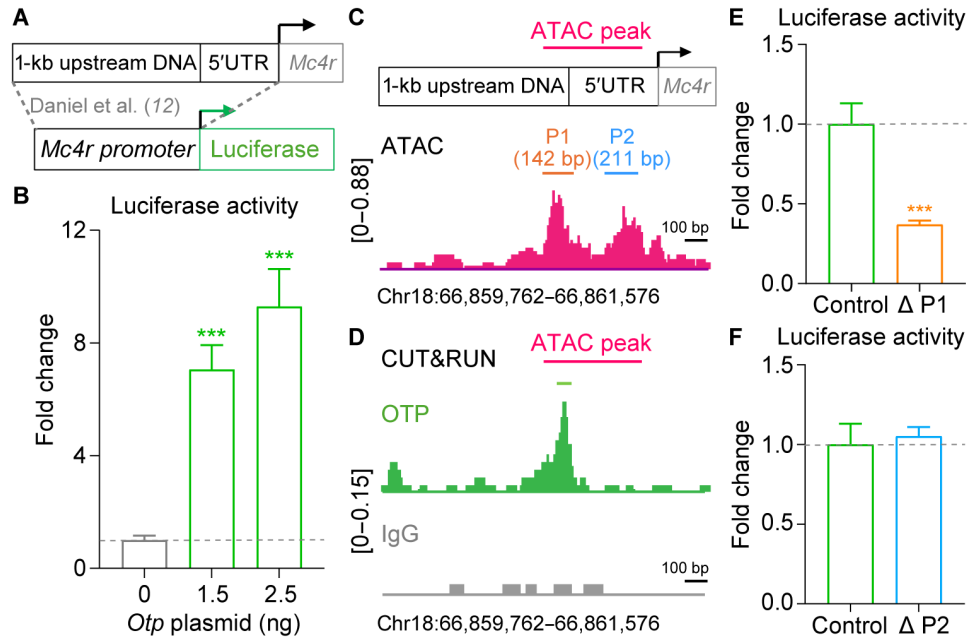
CUT&RUN peak was located within the P1 promoter sequence (Fig. 2, C and D). We generated luciferase reporter constructs lacking either the P1 or P2 sequence within the *Mc4r* promoter (ΔP1 and ΔP2 promoter, respectively). Cotransfection experiments revealed that the luciferase activity was significantly reduced with the ΔP1 promoter ($P < 0.001$; Fig. 2E) but unchanged with the ΔP2 promoter ($P > 0.05$; Fig. 2F).

Reduced *Otp* expression in developing PVN neurons causes weight gain

To investigate the physiological role of *Otp* in PVN neurons, we developed a floxed *Otp* allele (*Otp^fl*), which could be excised in the presence of *Cre* recombinase, resulting in a deleted allele (*Otp^Δ*; fig. S3, A to C). Similar to *Otp* nulls (*14*), mice homozygous for the deleted allele (*Otp^Δ/Δ*) die shortly after birth. On the other hand, quantitative polymerase chain reaction (qPCR) analyses found comparable expression of *Otp* mRNA within the hypothalami of *Otp^+/+*, *Otp^fl/+*, and *Otp^fl/fl* littermates (fig. S3D), suggesting that the introduced *loxP* sequences did not perturb *Otp* transcription.

PVN neurons express the TF *single-minded 1* (*Sim1*) (*15*). To ablate *Otp* in these neurons, we bred *Sim1-Cre* mice with *Otp^fl/fl* mice. Loss of *Otp* in *Sim1-Cre* neurons alone resulted in perinatal lethality; the PVN failed to form in *Sim1-Cre; Otp^fl/fl* mice (designated hereafter as *Otp^Sim1 KO* mice; Fig. 3A). In wild-type mice, the PVN contains abundant *Sim1*-expressing neurons at postnatal day 0. In contrast, these neurons were absent from the prospective PVN in *Otp^Sim1 KO* mice (Fig. 3A) but present in mice lacking one copy of *Otp* in *Sim1* neurons (*Sim1-Cre; Otp^fl/+*, designated hereafter as *Otp^Sim1 KD*; Fig. 3A). Cell counting in adult *Otp^Sim1 KD* mice revealed a normal number of PVN *Sim1-Cre* neurons along the rostral-to-caudal axis (fig. S4, A and B). Nevertheless, mRNA expression of *Otp* and *Mc4r* was reduced in the PVN (Fig. 3B and fig. S4C), whereas the expression of *Sim1* remained constant (Fig. 3C). Although *Otp^Sim1 KD* mice were viable and fertile, their body weights began to diverge on a chow diet. The weight gain was exacerbated

when mice were switched to a high-fat diet (HFD; Fig. 3D) and was characterized by increased fat mass (Fig. 3E) measured by nuclear magnetic resonance (NMR). Moreover, HFD-fed *Otp^Sim1 KO* mice consumed significantly more food than their littermate controls ($P < 0.001$; Fig. 3F).

### Loss of *Otp* in mature PVN neurons causes obesity

We next investigated whether *Otp* in PVN neurons regulates body weight beyond developmental stages. To this end, we bilaterally injected adeno-associated viruses (AAVs) expressing either *Cre* or green fluorescent protein (GFP) into the PVNs of adult *Otp^fl/fl*; *Ai14* mice (fig. S5A). Three weeks after the injection, we observed the expression of GFP or a Cre-activated tdTomato reporter in most PVN neurons (fig. S5B). Injections of *Cre*-expressing viruses resulted in a near-complete loss of Otp protein in the PVN (*Otp^PVN KO*; fig. S5B). Despite the absence of *Otp*, tdTomato-positive neurons persisted in the PVN (fig. S5B), indicating that *Otp* is not required for their survival in adulthood.

After the loss of *Otp*, mice on a chow diet gained excessive weight (Fig. 4A) and became obese with increased fat mass (Fig. 4B). Of note, this phenomenon was not observed in wild-type mice that received *AAV-Cre* in the PVN (fig. S5C). Metabolic chamber analyses revealed that *Otp^PVN KO* mice had increased food intake during the dark phase of the day (Fig. 4C) with no significant changes in heat production or physical activity ($P ≥ 0.05$; Fig. 4, D and E). These findings are consistent with previous reports that MC4R in the PVN preferentially regulates food intake (*6, 7*), whereas MC4Rs in other brain regions modulate energy expenditure (*16, 17*).

To unravel the molecular basis of weight gain, we isolated PVN neurons targeted with AAV-GFP or AAV-*Cre* by FACS and compared their transcriptomes using RNA-seq. Principal components analysis revealed that the loss of *Otp* altered the transcriptomic landscape in adult PVN neurons (fig. S6A); 1283 genes were down-regulated, whereas 576 were up-regulated (log$_2$FC > 1 and FDR <0.05; fig. S6B). Pathway analyses indicated deficits in hormone

Xu *et al.*, *Sci. Transl. Med.* **17**, eadr6459 (2025)   15 January 2025

3 of 11

Fig. 3. Reduced *Otp* in developing PVN neurons causes obesity. (**A**) Left: immunostaining of Otp. Right: fluorescence of tdTomato in *Sim1-Cre* (top), *Otp^{Sim1 KO}* (middle), and *Otp^{Sim1 KD}* (bottom) mice. White arrowheads point to the prospective PVN. Scale bar, 500 μm. (**B** and **C**) RNAscope analyses of PVN *Mc4r* (B) and *Sim1* (C) mRNAs in control and *Otp^{Sim1 KD}* mice. Scale bars, 50 μm. (**D**) Body weight curves of male mice. Two-way ANOVA with Šidák's post hoc test, $F_{1,240} = 80.56$, $P < 0.001$. (**E**) Body composition by NMR; two-way ANOVA with Šidák's post hoc test, $F_{1,26} = 12.96$, $P < 0.01$. (**F**) Food intake in HFD-fed mice; unpaired t test. Data are presented as means ± SEM. $*P < 0.05$, $**P < 0.01$, and $***P < 0.001$.
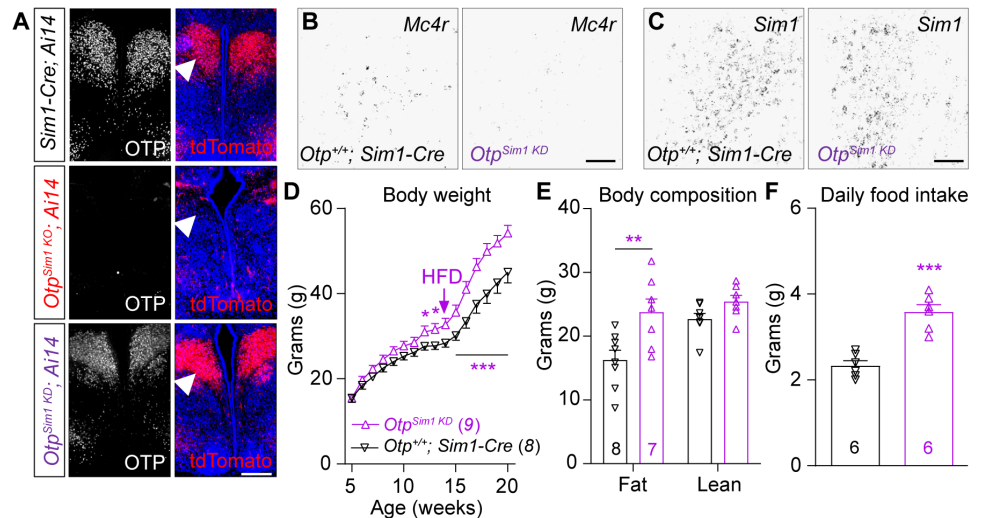
binding and peptide receptor activity (fig. S6C). PVN neurons synthesize and secrete several neuropeptides and hormones. Notably, others have shown that *Otp* is necessary for somatostatin (*Sst*) expression in the AN of the hypothalamus (*18*). We observed a similar reduction in *Sst* expression after the deletion of *Otp* in the adult PVN (Fig. 4F). In addition, mRNA expression of *Mc4r* and *oxytocin* (*Oxt*) was significantly reduced. Conversely, the expression of *Sim1* remained unchanged (Fig. 4, F and G, and fig. S5D). Alongside the alterations in the transcriptome, ATAC-seq experiments revealed diminished chromatin accessibility in the PVNs of *Otp^{PVN KO}* mice (fig. S6D). Consistent with the changes in gene expression, there was a significant decrease in ATAC peaks upstream of *Sst* (FDR = 0.05), *Mc4r* (FDR < 0.01), and *Oxt* (FDR = 0.01) after adult deletion of *Otp*, whereas those for *Sim1* (FDR > 0.05) remained unchanged (Fig. 4H).

Otp in *Mc4r-Cre* neurons regulates *Mc4r* expression and body weight

Deficiencies in PVN *Mc4r* (*6*, *7*) and *Oxt* (*19*, *20*) have been linked to hyperphagic obesity. *Otp* is present in both *Mc4r* and *Oxt* neurons within the PVN, and the expression of both genes decreased after the loss of *Otp*. However, we found that *Mc4r* and *Oxt* were expressed by largely nonoverlapping neurons in the PVN, with less than 1% of *Mc4r-Cre* neurons expressing *Oxt* (5 of the 734 neurons in two mice; fig. S7A). These findings suggest that *Otp* may regulate food intake and body weight in either *Mc4r*, *Oxt* neurons, or possibly both.

To investigate these possibilities, we generated *Otp^{Mc4r KO}* mice, in which *Otp* was selectively deleted from *Mc4r-Cre* neurons (fig. S7B), and *Otp^{Oxt KO}* mice, in which *Otp* was selectively deleted from neurons expressing *Oxt-Cre* (fig. S7C) (*21*). Chow-fed *Otp^{Mc4r KO}* mice were heavier at weaning (fig. S8A). In addition, when weight-matched mice were challenged with a HFD, male and female *Otp^{Mc4r KO}* mice gained significantly more weight due to increased adiposity and exhibited reduced glucose tolerance compared with controls (*P* < 0.001; Fig. 5, A to C, and fig. S8, B to D). In contrast, the deletion of *Otp* in *Oxt-Cre* neurons had no impact on these metabolic parameters (*P* > 0.05; Fig. 5, D to F). Collectively, these findings establish *Mc4r* neurons as a critical node where *Otp* regulates

energy balance. *Otp^{Mc4r KO}* mice consumed more food than controls (Fig. 5G). Moreover, mRNA expression of *Mc4r* was reduced in the PVNs of *Otp^{Mc4r KO}* mice, whereas *Oxt* expression did not change (Fig. 5H and fig. S8E). In addition, male and female *Otp^{Mc4r KO}* mice exhibited increased body length compared with littermate controls (Fig. 5I and fig. S8F), a hallmark of *MC4R* deficiency in mice and humans (*22*).

Knock-in mouse model of a human LOF variant in *OTP* develops obesity

The protein sequences of *OTP* are highly conserved across mammalian species and are identical between mice and humans. We have previously identified rare variants in *OTP* in children with severe obesity (*23*). Here, to investigate whether coding variants in *OTP* are associated with body mass index (BMI) in a population-based biobank, we examined 454,756 individuals with exome sequence data from the UK Biobank (UKB) study. Five UKB participants had a heterozygous predicted LOF (pLOF) variant in *OTP*. Four had obesity (BMI > 30 kg/m²) at UKB assessment (*n* = 4 of 5, 80% compared with 24% of unrelated white British people (*n* = 318,365; odds ratio of 12.6, 95% confidence interval of 1.2 to 617, *P* = 0.01, Fisher's exact test). Although these data are suggestive of an association, studies in larger cohorts will be needed to formally test whether LOF variants in *OTP* increase BMI or the risk of developing obesity.

To determine whether there is a causal link between human *OTP* mutations and obesity, we generated knock-in mice carrying the heterozygous missense mutation *Otp^{Q153R/+}*, previously identified in a child with severe obesity (BMI SD score of 4.6 at 2 years) (*23*). The proband experienced progressive weight gain during adolescence and developed type 2 diabetes, dyslipidemia, and hepatic steatosis. The amino acid Q153 resides in the DNA-binding domain and is highly conserved across multiple species (fig. S9A). We generated *Otp^{Q153R/+}* mice derived from two independent founder lines (fig. S9B). In these mice, Sanger sequencing identified cDNA encoding wild-type and mutant *Otp* transcripts in the hypothalamus (fig. S9C). Like *Otp* nulls (*Otp^{Δ/Δ}*), mice homozygous for the mutant allele (*Otp^{Q153R/Q153R}*) died shortly after birth. Moreover, *Otp^{Q153R}* failed to rescue lethality in the compound heterozygous *Otp^{Q153R/Δ}*
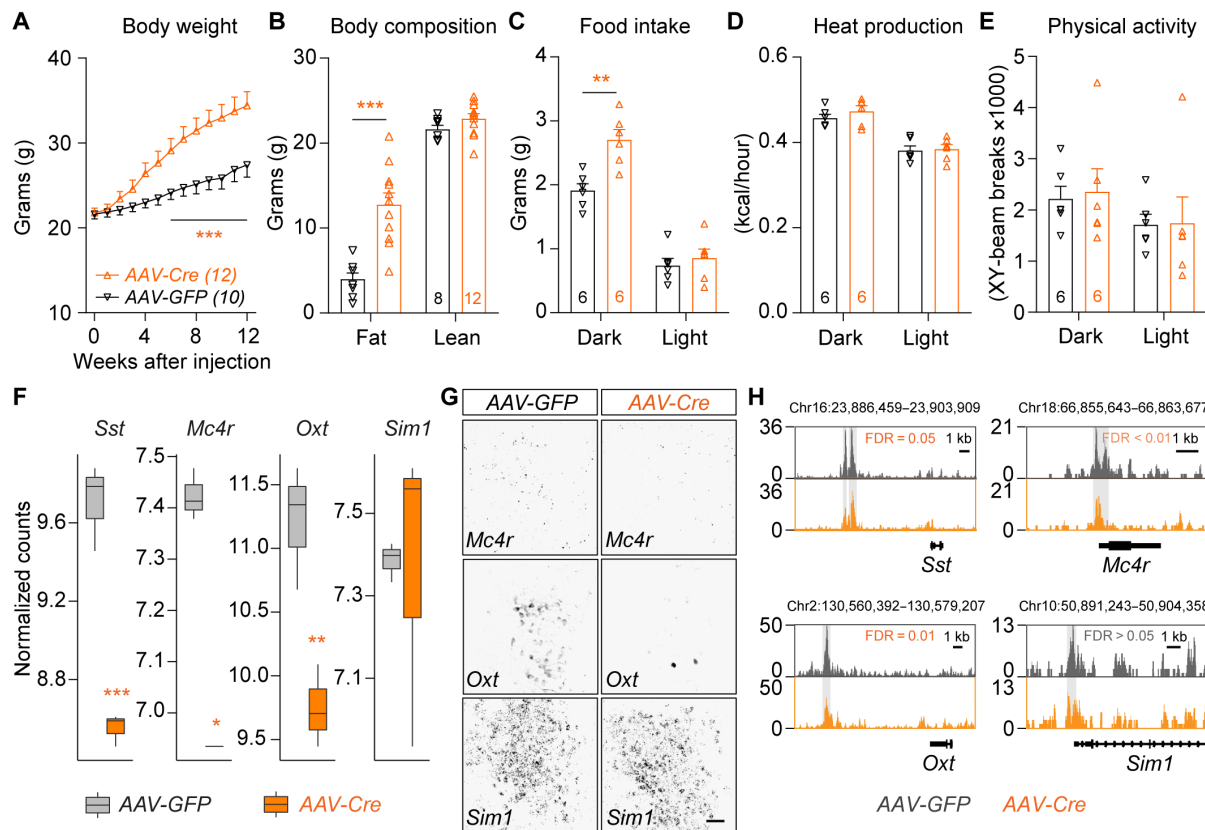
Fig. 4. Loss of *Otp* in adult PVN leads to weight gain. (**A**) Body weight curves in *Otp*[PVN KO] mice; two-way ANOVA with Šidák's post hoc test, $F_{1,20} = 7.72$, $P = 0.01$. (**B**) Body composition; two-way ANOVA with Šidák's post hoc test, $F_{1,34} = 26.91$, $P < 0.001$. (**C**) Food intake; two-way ANOVA with Šidák's post hoc test, $F_{1,10} = 13.33$, $P < 0.01$. (**D**) Heat production; two-way ANOVA with Šidák's post hoc test, $F_{1,10} = 0.57$, $P = 0.47$. (**E**) Physical activity; two-way ANOVA with Šidák's post hoc test, $F_{1,10} = 0.03$, $P = 0.87$. (**F**) Normalized RNA-seq reads of individual genes between AAV-GFP– and AAV-Cre–targeted PVN neurons. *FDR < 0.05, **FDR < 0.01, and ***FDR < 0.001. (**G**) RNAscope analyses of *Mc4r*, *Oxt*, and *Sim1* mRNAs in the PVN. Scale bar, 50 μm. (**H**) Genome browser views of representative ATAC-seq peaks upstream of *Sst*, *Mc4r*, *Oxt*, and *Sim1* in control and *Otp*[PVN KO] mice. Data are presented as means ± SEM. *P < 0.05, **P < 0.01, and ***P < 0.001.

mice. Collectively, these data suggest that *Otp*[Q153R] encodes a LOF mutation.

Heterozygous mutant mice (*Otp*[Q153R/+]) survived throughout adulthood. At 10 weeks of age, male and female *Otp*[Q153R/+] mice on a chow diet were heavier than their wild-type littermates (fig. S9D). Moreover, they gained significantly more weight when fed a HFD (*P* < 0.001; Fig. 6, A and B), resulting in excessive lipid accumulation in the white adipose tissue and liver (Fig. 6C). Metabolic chamber analyses of weight-matched *Otp*[Q153R/+] and *Otp*^{+/+} mice showed that, although food intake was comparable in chow-fed mice, *Otp*[Q153R/+] mice consumed significantly more food after switching to the HFD (*P* < 0.001; Fig. 6D). Moreover, there was no difference between the genotypes in heat production or physical activity before or after the change in diet (Fig. 6, E and F). In addition, HFD-fed *Otp*[Q153R/+] mice exhibited impaired glucose tolerance and insulin sensitivity concomitant with their obesity (Fig. 6, G and H).

Mc4r insufficiency contributes to weight gain in *Otp*[Q153R/+] mice

To dissect the cellular and molecular deficits causing weight gain in *Otp*[Q153R/+] mice, we generated triple transgenic mice (*Sim1-Cre; Sun1-sfGFP; Otp*[Q153R/+]) where PVN neurons in these mice were genetically labeled by the expression of a nuclear GFP (Sun1-sfGFP).

Histological analyses indicated that the PVN developed normally in *Otp*[Q153R/+] mice with a comparable number of *Sim1-Cre* neurons to wild-type controls (Fig. 7A). Next, we purified GFP+ nuclei from PVN *Sim1-Cre* neurons by FACS and conducted single-nucleus RNA-seq (snRNA-seq) to examine neuronal subtypes and their gene expression profiles in age-matched *Otp*^{+/+} and *Otp*[Q153R/+] mice (Fig. 7A). We analyzed the transcriptomes of 2695 *Sim1* positive nuclei, with an average of 2477 detected genes per nucleus. These data allowed us to identify nine distinct subgroups among PVN *Sim1* neurons marked by the expression of neuroendocrine markers, such as *Sst*, *Oxt*, or *Crh* (Fig. 7B and fig. S10A). Although there were no genotypic differences in cell numbers among individual subpopulations (Fig. 7C and fig. S10B), the expression of *Mc4r*, *Oxt*, and *Sst* decreased in *Otp*[Q153R/+] mice, whereas that of *Sim1* remained unchanged (Fig. 7, D and E).

Our findings suggest that hyperphagia and obesity in mice expressing a human LOF *OTP* mutation may result, in part, from reduced MC4R signaling. Setmelanotide, a selective MC4R agonist, has been licensed for the chronic weight management of people with three genetic obesity disorders (*24*). We previously demonstrated that an intraperitoneal dose of setmelanotide (2 mg/kg) suppressed fasting-induced refeeding in wild-type mice but not those lacking *Mc4r* in PVN neurons (*6*). Here, we fed male *Otp*[Q153R/+]

Fig. 5. *Otp* in *Mc4r-Cre* neurons regulates energy and glucose homeostasis. (**A**) Body weight curves in HFD-fed male *Otp*^{Mc4r KO} mice; two-way ANOVA with Šidák's post hoc test, $F_{1,18} = 23.71$, $P < 0.001$. (**B**) Body composition; two-way ANOVA with Šidák's post hoc test, $F_{1,18} = 23.56$ $P < 0.001$. (**C**) GTT; two-way ANOVA with Šidák's post hoc test, $F_{1,54} = 79.79$, $P < 0.001$, $n = 5$ or 6. (**D**) Body weight curves in HFD-fed male mice; two-way ANOVA, $F_{1,18} = 1.61$, $P = 0.22$. (**E**) Body composition; two-way ANOVA with Šidák's post hoc test, $F_{1,18} = 1.88$, $P = 0.19$. (**F**) GTT; two-way ANOVA with Šidák's post hoc test, $F_{1,18} = 0.03$, $P = 0.87$, $n = 9$ to 11. (**G**) Daily food intake in HFD-fed mice; unpaired t test. (**H**) RNAscope analyses of *Oxt* and *Mc4r* mRNAs in the PVN. Scale bar, 50 μm. (**I**) Body length; unpaired t test. Data are presented as means ± SEM. **$P < 0.01$ and ***$P < 0.001$.
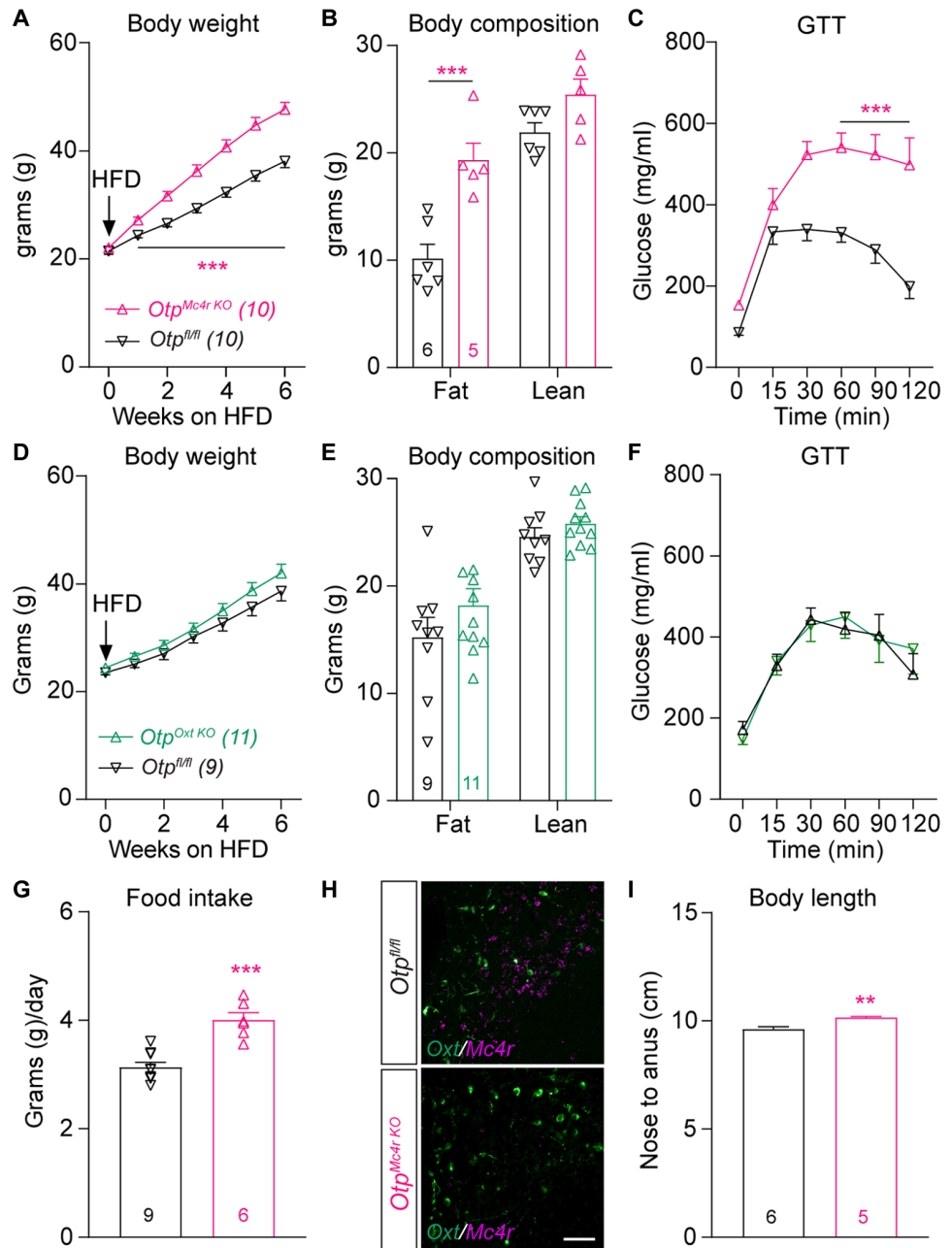

mice a HFD for 10 weeks. Obese mice (>40 g) with similar weights were then divided into two groups, one treated with setmelanotide and the other with vehicle (saline), while both were still on the HFD (Fig. 7F). Using the same dose, daily single injections of setmelanotide in HFD-fed *Otp*^{Q153R/+} mice reduced their body weights by 6.63 ± 1.04% after 9 days. In contrast, those treated with saline gained 1.79 ± 0.54% more weight during the same period (Fig. 7G). During treatment, food intake was reduced in *Otp*^{Q153R/+} mice (Fig. 7H). In addition, these mice exhibited improved glucose tolerance (Fig. 7I). Notably, these metabolic benefits were contingent on continued setmelanotide treatment because *Otp*^{Q153R/+} mice quickly regained body weight after the treatment was discontinued (Fig. 7J).

DISCUSSION

Our studies reveal that *Otp* is a transcriptional regulator of *Mc4r* in PVN neurons. We show that disruption of *Otp* in developing and adult mice causes increased food intake and obesity, findings that were recapitulated in a knock-in mouse model of a rare LOF human variant in *OTP*, demonstrating their relevance for the regulation of human energy homeostasis. LOF mutations in *OTP* are very rare, with no homozygous mutations identified in 2000 children with severe obesity or 0.5 million people in UKB, which aligns with the observation that mice lacking *Otp* do not survive. Our analysis of UKB data identified people carrying rare heterozygous pLOF variants in the general population; four of five had obesity. How these

Xu et al., Sci. Transl. Med. **17**, eadr6459 (2025)   15 January 2025

6 of 11

Fig. 6. $Otp^{Q153R/+}$ mice develop obesity and glucose intolerance. (**A**) Body weight curves in HFD-fed mice; two-way ANOVA with Šidák's post hoc test, $F_{1,562} = 161.1$, $P < 0.001$. (**B**) Body composition; two-way ANOVA with Šidák's post hoc test, $F_{1,12} = 20.69$, $P < 0.001$. (**C**) Hematoxylin and eosin (H&E) staining in the livers and inguinal white adipose tissue (iWAT) of HFD-fed $Otp^{+/+}$ and $Otp^{Q153R/+}$ mice. Scale bar, 50 µm. (**D**) Left are traces of continuous measurement of cumulative food intake in metabolic cages (binned into 12-hour light and dark phases) before and after the dietary switch (red dashed line); right are summarized daily averages of food intake. Two-way ANOVA with Šidák's post hoc test, $F_{1,10} = 10.23$, $P = 0.01$. (**E**) Left are traces of continuous measurement of heat production in metabolic cages; right are summarized daily averages of heat production. Two-way ANOVA with Šidák's post hoc test, $F_{1,10} = 0.34$, $P = 0.58$. (**F**) Left are traces of continuous measurement of physical activity in metabolic cages; right are summarized daily averages of physical activity. Two-way ANOVA with Šidák's post hoc test, $F_{1,10} = 0.39$, $P = 0.55$. (**G**) GTT; two-way ANOVA with Šidák's post hoc test, $F_{1,66} = 42.03$, $n = 6$ or 7, $P < 0.001$. (**H**) ITT; two-way ANOVA with Šidák's post hoc test, $F_{1,66} = 22.04$, $P < 0.001$, $n = 6$ or 7. Data are presented as means ± SEM. *$P < 0.05$, **$P < 0.01$, and ***$P < 0.001$.
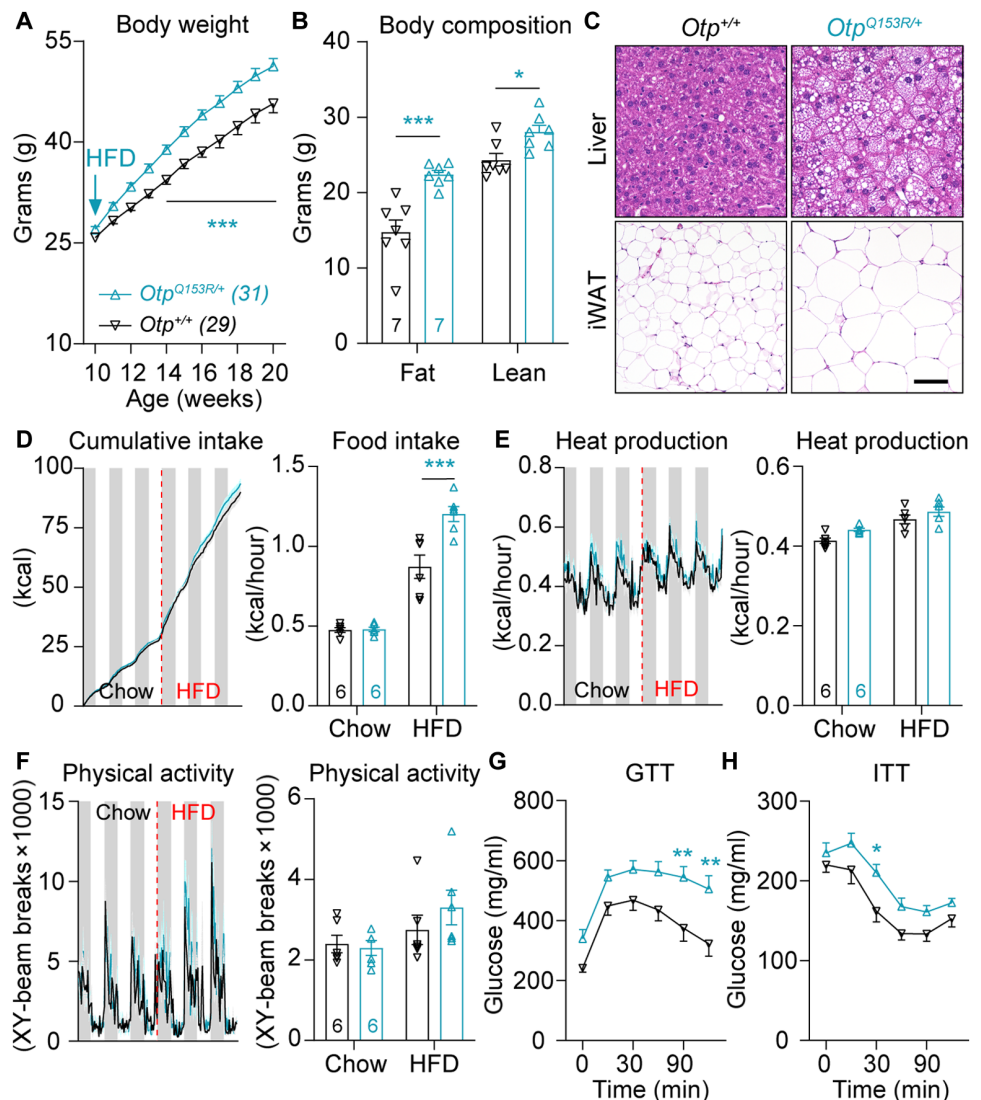
pLOF mutations impair OTP function and MC4R expression remains to be determined. Moreover, future studies in even larger cohorts are warranted to formally test whether other functional variants in *OTP* are associated with increased BMI and/or the risk of developing obesity.

Before our study, how LOF *OTP* mutations drive excessive weight gain was unclear. We and others have shown previously that *Otp* is necessary for the generation of several neuroendocrine lineages in the PVN (*23*, *25*). With one copy of *Otp*, although a normal number of PVN neurons were preserved in $Otp^{Sim1\ KD}$ and $Otp^{Q153R/+}$ mice, the expression of *Mc4r* was diminished along with that of *Sst* and *Oxt*. Whereas *Sst* null mice demonstrate normal body weight and length (*26*), oxytocin deficiency in the PVN has been implicated in obesity (*19*). In addition, despite a reduction in *Oxt* expression, $Otp^{Oxt\ KO}$ mice exhibited normal body weights and body fat levels even when challenged with a HFD. In contrast, loss of *Otp* in *Mc4r-Cre* neurons led to early-onset obesity, excessive weight gain, and increased body length, characteristic of *MC4R* deficiency in mice and humans. Collectively, these findings establish a cell-autonomous role for *Otp* in *Mc4r* neurons to regulate *Mc4r* expression and body weight. However, it is possible that *Otp* also

regulates energy balance by acting in other neuronal populations or through mechanisms beyond the regulation of *Mc4r* transcription.

Our study has several limitations. Although our data suggest that obesity in humans with LOF *OTP* mutations is at least in part mediated by reduced MC4R signaling, additional mechanisms may also be involved. We generated $Otp^{Q153R/+}$ mice to study a human LOF variant in *OTP*. However, as with all preclinical models, this mouse model may not fully replicate the phenotype of human *OTP* deficiency. In addition, our research focused primarily on changes in food intake and body weight; we did not examine the impact of the OTP mutation on other physiological functions and behaviors. Last, although we demonstrated that treatment with a licensed MC4R agonist reduced body weights in mice, these findings require validation in the clinical setting.

Beyond neurodevelopment, adequate abundance of MC4R must be maintained throughout life to maintain energy homeostasis. However, transcriptional programs that regulate *Mc4r* expression in the adult brain remain essentially unknown. Our findings indicate that the transcriptional regulation of *Mc4r* is complex and region-specific: No identified TFs are expressed by all *Mc4r* neurons in the

Fig. 7. Setmelanotide treatment reduces obesity and glucose intolerance in $Otp^{Q153R/+}$ mice. (**A**) Genetic labeling of $Sim1$-Cre^+ nuclei with a nuclear GFP in $Otp^{+/+}$ and $Otp^{Q153R/+}$ mice. Inset: GFP fluorescence showing a normal number of $Sim1$-Cre neurons present in the PVNs of adult $Otp^{Q153R/+}$ mice. Scale bar, 50 μm. (**B**) Transcriptome-based dimensionality reduction analyses (Uniform Manifold Approximation and Projection; UMAP) in 2695 PVN $Sim1^+$ nuclei identified nine neuronal clusters. $Adarb2$, adenosine deaminase RNA–specific B2; Avp, arginine vasopressin; Crh, corticotropin-releasing hormone; Oxt, oxytocin; Sst, somatostatin; $Tenm2$, teneurin transmembrane protein 2; Trh, thyrotropin-releasing hormone; $Agtr1a$, angiotensin II receptor, type 1a; $Bdnf$, brain-derived neurotrophic factor; $Ucn3$, urocortin 3. (**C**) Bar graphs showing the distribution of PVN $Sim1^+$ nuclei across individual neuronal clusters in $Otp^{+/+}$ and $Otp^{Q153R/+}$ mice. Chi-square test, $P = 0.23$. (**D**) Dot plots showing the relative expression of $Mc4r$, Sst, and Oxt in PVN $Sim1$ neurons of $Otp^{+/+}$ and $Otp^{Q153R/+}$ mice. Dot size reflects the relative number of cells expressing a gene of interest (normalized to the values in $Otp^{+/+}$ mice), and color intensity reflects the relative expression (darker, more highly expressed). (**E**) RNAscope analyses of $Mc4r$ and $Sim1$ mRNAs in the PVNs of $Otp^{+/+}$ and $Otp^{Q153R/+}$ mice. Scale bar, 50 μm. (**F**) Schematic for treating $Otp^{Q153R/+}$ mice with vehicle or SET (setmelanotide) after diet-induced obesity. (**G**) Changes in body weight before and after the 9-day treatment with vehicle or SET; $n = 7$ or 8, paired t test. (**H**) Cumulative food intake in $Otp^{Q153R/+}$ mice treated with vehicle or SET. The gray area indicates the 9-day treatment period; two-way ANOVA with Šidák's post hoc test, $F_{1,10} = 8.19$, $P < 0.05$. (**I**) GTT; two-way ANOVA with Šidák's post hoc test, $F_{5,65} = 2.259$, $P < 0.05$. (**J**) Changes in body weight after the treatment with vehicle or SET; $n = 7$ or 8; vehicle-treated $Otp^{Q153R/+}$ mice gained 1.16 ± 0.24 g, whereas SET-treated $Otp^{Q153R/+}$ mice gained 3.31 ± 0.31 g; paired t test, $P < 0.001$. Data are presented as means ± SEM. $*P < 0.05$ and $***P < 0.001$.
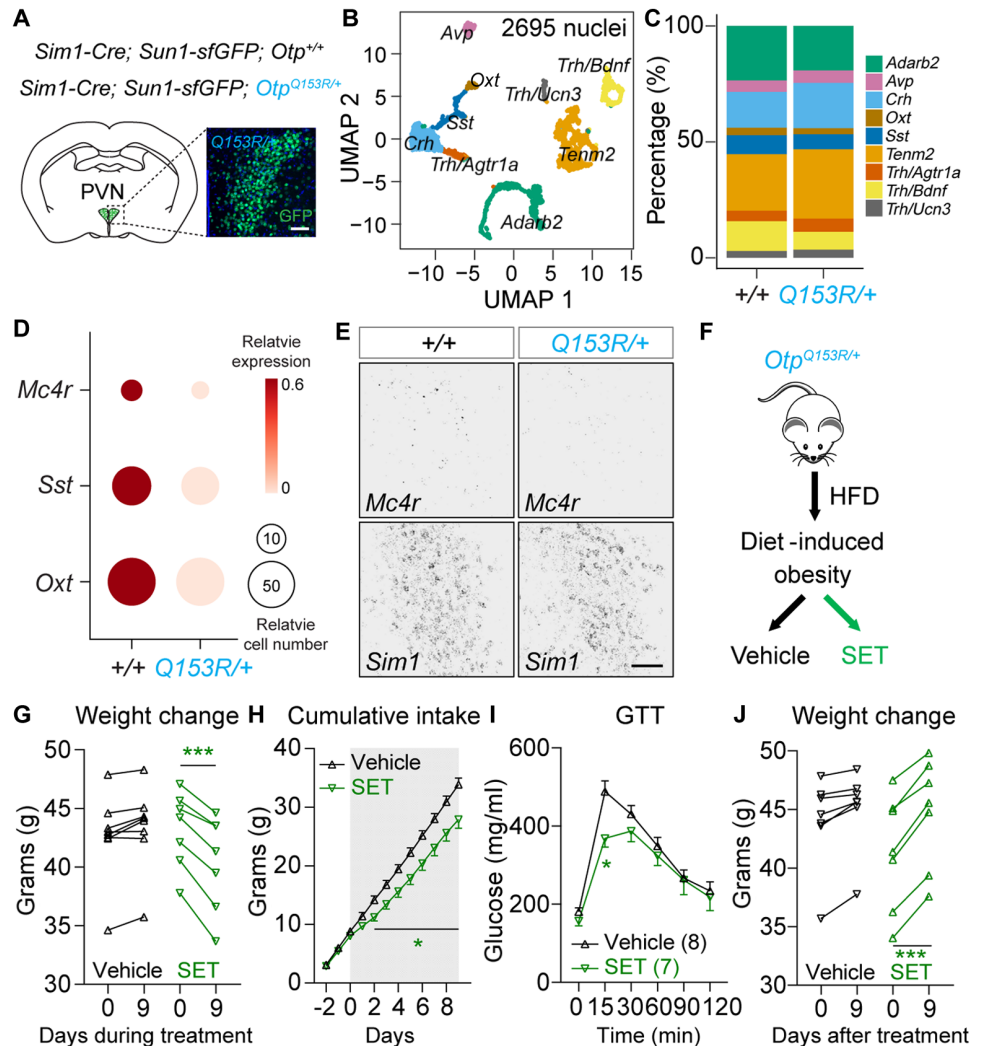
hypothalamus. We demonstrate that Otp is one of the transcriptional regulators maintaining $Mc4r$ expression in the adult PVN. However, even in the absence of Otp, residual $Mc4r$ persists, indicating the involvement of additional coregulators. For instance, $Foxp2$ is found in a subset of PVN $Mc4r$ neurons. Moreover, $Sim1$ and $Nescient helix-loop-helix 2$ ($Nhlh2$), a basic helix-loop-helix protein, are present in the adult PVN and play important roles during neurodevelopment (27, 28). However, whether they regulate $Mc4r$ transcription in mature PVN neurons remains to be determined.

Whereas previous human studies have primarily focused on deficits in MC4R signaling (5, 29), our findings suggest that human obesity may also result from deficits in $MC4R$ transcription. Studies in mice and humans have demonstrated a genotype-phenotype correlation between $Mc4r$ function and the severity of obesity (5, 22). We observed a similar dosage effect with $Mc4r$ in the four Otp knock-out/knock-down mouse models: Deletion of both copies of Otp in PVN neurons resulted in an ~50% reduction in $Mc4r$ in the PVN, leading to early-onset obesity (in $Otp^{Mc4r\ KO}$ mice) and rapid weight gain in chow-fed adult mice (in $Otp^{PVN\ KO}$ mice). In comparison, the reduction in $Mc4r$ expression

was less pronounced when one functional copy of Otp still existed; weight gain was moderate in chow-fed $Otp^{Sim1\ KD}$ and $Otp^{Q153R/+}$ mice but exacerbated when they were fed a HFD. The residual $Mc4r$ expression in the PVN and other neurons may explain the substantial weight loss in $Otp^{Q153R/+}$ mice treated with setmelanotide. These findings suggest that people carrying functional mutations in OTP may benefit from treatment with a licensed MC4R agonist. Last, although therapeutic targeting of TFs has historically been challenging, small-molecule modulators of TF activity are now being developed in other disease areas (30). Thus, understanding the transcriptional regulation of molecules involved in energy homeostasis may reveal targets for the development of anti-obesity medication.

MATERIALS AND METHODS
Study design
This study investigated the transcriptional regulation of $Mc4r$ in the mouse hypothalamus. We used neuroanatomical characterization, mouse genetics, and transcriptomic analyses to explore the role of

Otp in controlling *Mc4r* expression and body weight. In addition, we examined the functional impact of a human LOF OTP mutation in mice. All experimental procedures in mice were approved by the Institutional Animal Care and Use Committee (IACUC) at the University of Texas Southwestern Medical Center. All experiments were conducted in the inbred C57BL/6J mouse strain because this strain is the most commonly used mouse strain for the study of feeding behavior and energy homeostasis. Both sexes were used as experimental animals and randomly assigned to groups. We replicated experiments at least once to ensure biological reproducibility and adequate statistical analysis for comparisons.

All clinical studies in humans were approved by the Multi-Regional Ethics Committee and the Cambridge Local Research Ethics Committee (MREC 97/21 and REC number 03/103). Each participant (or their parent for those under 16 years old) provided written informed consent; minors provided oral consent. All studies were conducted in accordance with the Declaration of Helsinki. Exome sequencing studies were undertaken as described previously (*31*, *32*).

UKB 450K exomes

This research was conducted using the UKB Resource under Application Number 53821. Variants in the *OTP* gene region (ENSG00000171540) were obtained from the UKB 450K exome release in pVCF format (UKB Field 23148). Variant annotation was performed using Ensembl Variant Effect Predictor (VEP; Ensembl release 110) for consequences with respect to Ensembl transcript ENST00000306422.5. We defined predicted high-impact or truncating (pLOF) variants in *OTP* as stop-gained, frameshift, splice donor, or acceptor variants. BMI (kilograms per square meter) was from the UKB initial assessment visit (UKB Field 21001, Instance 0) as were age (Field 21003), genetic sex (Field 22001), and self-reported comparative body size at age 10 (Field 1687). For subgroup analysis among unrelated white British ancestry exomes, we obtained relatedness from the UKB Genetic Data resource (ukbgene rel) and excluded one person from each related pair (kinship ≥ 0.0442, KING, third-degree kinship, or closer) and exomes that were not in the UKB white British ancestry genetic grouping (UKB Field 22006).

Mouse strains

All mice were housed in a temperature and humidity-controlled room with a 12-hour-light/dark cycle (lights on at 6:00 a.m., lights off at 6:00 p.m.) in the animal facility of the University of Texas Southwestern Medical Center. Food and water were supplied ad libitum. Mice were fed with either regular chow (4.25% kcal from fat; Harlan-Teklad, Madison, WI, no. 2916) or a HFD (60% kcal from fat; Research Diets Inc., no. D12492i). Commercial mouse lines were C57BL/6J wild type (JAX, no. 000664), *Mc4r-Cre* [JAX, no. 030759 (*8*)], *Sim1-Cre* [JAX, no. 006395 (*7*)]; *Oxt-Cre* [JAX, no. 024234 (*21*)], *Rosa26-Ai14-CAG-LSL-TdTom* [JAX, no. 007914 (*9*)], and *Rosa26- CAG-Sun1/sfGFP* [JAX, no. 021039 (*33*)]; *Rosa26-Ai75-CAG-nls-TdTom* [JAX, no. 025106 (*34*)] mice were purchased from Jackson Laboratory. *Otp*^fl/fl^ and *Otp*^Q153R/+^ mice were generated by CRISPR-Cas9–mediated gene editing at the fertilized one-cell stage.

Generation of *Otp*^fl/fl^ and *Otp*^Q153R/+^ mice with CRISPR-Cas9–based genome editing

LoxP sites were inserted, flanking exon 3 of the mouse *Otp* gene. Two 20-bp single-stranded DNA Ultramer DNA oligomers [Integrated

DNA Technologies (IDT)] containing a loxP site flanked by ~80-bp homology arms were used as homology directed repair (HDR) templates. Guide RNAs, tracerRNA, Cas9 protein, and HDR templates were ordered from IDT. Mice were screened and validated by PCR and Sanger sequencing. Recombination of the allele was verified by crossing mice to a germline Cre. To introduce the Q153R mutation, two bases in exon 3 were mutated from CAG to CGA. The *Otp* gene was targeted using the following guide sequence: 5′-GACCCTGCTCGCTAACC-TCG TGG-3′. Guide RNAs, tracerRNA, Cas9 protein, and HDR template were ordered and injected into C57BL/6 zygotes by the UT Southwestern Transgenic Technology Center. Founders were screened by Sanger sequencing.

Body weight, composition, and length measurements

Body weight was monitored weekly from weaning (4 weeks old) up to 20 weeks of age. Body composition was assessed using the Bruker Minispec mq10 NMR analyzer at the end of the body weight monitoring. Body length (nose to anus distance in centimeters) was measured by extending the mouse to its full length after anesthesia.

H&E staining

Mouse adipose tissues were fixed in 4% paraformaldehyde (Electron Microscopy Sciences, no. 15710S) overnight and then dehydrated through a series of ethanol baths with ascending concentrations (up to 100%). The Histo Pathology Core of the UT Southwestern Medical Center performed paraffin embedding, sectioning, and hematoxylin and eosin (H&E) staining.

Immunostaining and RNAscope

Details for performing these experiments were described previously (*35*). Briefly, mouse brains were fixed in 4% paraformaldehyde overnight and then were sectioned with a vibratome (Leica VT1000S). The primary antibodies used included anti-OTP (rabbit; Sigma-Aldrich, no. HPA039365), anti-GFP (rabbit; Abcam, no. ab290), anti–red fluorescent protein (rabbit; Rockland, no. 600-401-379), and anti-oxytocin (rabbit; ImmunoStar, no. 20068). The secondary antibodies (Alexa Fluor 488, Alexa Fluor 594, or Alexa Fluor 647) were from Thermo Fisher Scientific. RNAscope was performed using the ACD RNAscope Multiplex Fluorescent Detection Kit version 2 following the manufacturer's (Advanced Cell Diagnostics, no. 323270) protocol with the following probes: *Mm-Dlx5*, *Mm-Foxp2*, *Mm-Onecut2*, *Mm-Mc4r*, and *Mm-Sim1*.

qPCR analysis

Total PVN RNA was isolated with the Direct-zol RNA Kit (Zymo, no. R2050) according to the manufacturer's recommendations. Total RNA (~500 ng) was used as the template for cDNA synthesis via M-MLV reverse transcriptase (Invitrogen, no. 28025013). qPCR was performed using TaqMan universal PCR master mix (Thermo Fisher Scientific, no. 4444964). TaqMan probes included *Tbp* (Mm00446973_m1; Thermo Fisher Scientific, no. 4331182) as an internal control, *Mc4r* (Mm00457483_s1; Thermo Fisher Scientific, no. 4331182), *Oxt* (Mm01329577_g1; Thermo Fisher Scientific, no. 4331182), and a customized *Otp* exon3 probe (IDT). The probe sequence for *Otp* exon3 was 5′- CGCAAGAAGACCACCAACGTGTTC-3′. The forward primer was 5′-CGCGCCAAGTGGAAGAA-3′, and the reverse primer was 5′-GTGGAAAGAGCACAGGCT-3′. The relative expression of each gene was normalized to the housekeeping gene TATA-box binding protein (*Tbp*). RNA expression was quantified using the −ΔΔCt method.

Metabolic phenotype analysis

The acute effects of adult deletion of *Otp*, as well as *Otp*$^{Q153R/+}$, on energy intake and expenditure were measured using an indirect calorimetric system (PhenoMaster; TSE Systems) in the Metabolic Phenotyping Core of UT Southwestern Medical Center. For the set-melanotide studies, *Otp*$^{Q153R/+}$ mice were placed on a HFD to reach about 40 to 45 g. After that, the animals were singly housed for 3 days to acclimatize and to obtain baseline measurements for body weight and food intake. After acclimatization, animals were weighed and treated daily with saline or setmelanotide solution (2 mg/kg; Med-ChemExpress, no. HY-19870) via intraperitoneal injections. Animals were monitored for body weight and food intake daily during and 9 days after treatment. For the glucose tolerance test (GTT) and insulin tolerance test (ITT), mice were fasted for 7 hours with water provided ad libitum from 8:00 a.m. on the experimental day. During GTT, blood glucose concentrations were monitored at 0, 15, 30, 60, 90, and 120 min after an intraperitoneal dose of glucose [dextrose (AllMedTech, no. 00409664802); 1.0 g/kg body weight]. Blood glucose was taken from the tail vein and analyzed using a glucometer (Johnson & Johnson). For the ITT, blood glucose concentrations were monitored at 0, 15, 30, 60, 90, and 120 min after an intraperitoneal dose of insulin (Eli Lilly and Company, no. 0002-8215-01; 1 U/kg body weight).

Stereotaxic surgery

Male mice (~8 weeks old) were anesthetized with 1.5% isoflurane (Covetrus, no. 11695-6777-1) and placed on a stereotaxic frame (David Kopf Instruments). After the skull was exposed and leveled in the horizontal plane, small holes were drilled into the skull. AAV was bilaterally injected into the PVN (anteroposterior, −0.50 mm; mediolateral, ±0.22 mm; and dorsoventral, −4.80 mm). A total of 100 nl of the virus was injected in one side at a rate of 20 nl/min and was allowed 8 to 10 min to diffuse before the injection needle was removed. AAV vectors used included AAV8-hSyn-GFP (UNC Vector Core) and AAV8-hSyn-Cre-GFP (UNC Vector Core).

Plasmid construction

The pGL4.20-Mc4r-ΔP1-luc2 and pGL4.20-Mc4r-ΔP2-luc2 plasmids were constructed as follows: the Mc4r-ΔP1 and Mc4r-ΔP2 fragments were synthesized in vitro (IDT) and then subcloned into the pGL4.20-luc2 vector (Promega, no. E675A) using a homologous recombination kit (New England Biolabs, no. E5520S).

Luciferase activity assay

For measuring the *Mc4r* promoter activity, Neuro2A cells (American Type Culture Collection, no. CCL-131) were transiently cotransfected with a pCMV-Otp plasmid (OriGene Technologies, no. mr222320), a Renilla luciferase reporter, pCMV-Rluc (Promega, no. AF025843), and a respective *Mc4r* promoter construct (pGL3-Mc4r-Promoter-luc, which was a gift from K. G. Mountjoy; pGL4.20-Mc4r-ΔP1-luc2; and pGL4.20-Mc4r-ΔP2-luc2) via Lipofectamine 3000 reagent (Invitrogen, no. L3000008). The next day, trypsin (Sigma-Aldrich, no. 59417C)–dissociated cells were separated evenly into a 96-well plate. Luminescence was quantified using Dual-Glo luciferase assay (Promega, no. TM058).

Statistical analysis

Statistical tests, significance, and sample sizes are detailed in each figure legend. Statistical analyses were performed using GraphPad Prism 10.0 software. Data are presented as means ± SEM. Normality was tested before applying parametric tests. Statistical analyses were performed using unpaired two-tailed Student's *t* test and regular one-way or two-way analysis of variance (ANOVA). Differences with $P \leq 0.05$ were considered significant: *$P < 0.05$, **$P < 0.01$, and ***$P < 0.001$.

REFERENCES AND NOTES

1. P. Sweeney, L. E. Gimenez, C. C. Hernandez, R. D. Cone, Targeting the central melanocortin system for the treatment of metabolic disorders. *Nat. Rev. Endocrinol.* **19**, 507–519 (2023).
2. H. Krude, H. Biebermann, W. Luck, R. Horn, G. Brabant, A. Gruters, Severe early-onset obesity, adrenal insufficiency and red hair pigmentation caused by POMC mutations in humans. *Nat. Genet.* **19**, 155–157 (1998).
3. R. S. Jackson, J. W. Creemers, S. Ohagi, M. L. Raffin-Sanson, L. Sanders, C. T. Montague, J. C. Hutton, S. O'Rahilly, Obesity and impaired prohormone processing associated with mutations in the human prohormone convertase 1 gene. *Nat. Genet.* **16**, 303–306 (1997).
4. G. S. Yeo, I. S. Farooqi, S. Aminian, D. J. Halsall, R. G. Stanhope, S. O'Rahilly, A frameshift mutation in MC4R associated with dominantly inherited human obesity. *Nat. Genet.* **20**, 111–112 (1998).
5. L. A. Lotta, J. Mokrosinski, E. Mendes de Oliveira, C. Li, S. J. Sharp, J. Luan, B. Brouwers, V. Ayinampudi, N. Bowker, N. Kerrison, V. Kaimakis, D. Hoult, I. D. Stewart, E. Wheeler, F. R. Day, J. R. B. Perry, C. Langenberg, N. J. Wareham, I. S. Farooqi, Human gain-of-function MC4R variants show signaling bias and protect against obesity. *Cell* **177**, 597–607.e9 (2019).
6. L. Li, E. S. Yoo, X. Li, S. C. Wyler, X. Chen, R. Wan, A. G. Arnold, S. G. Birnbaum, L. Jia, J. W. Sohn, C. Liu, The atypical antipsychotic risperidone targets hypothalamic melanocortin 4 receptors to cause weight gain. *J. Exp. Med.* **218**, e20202484 (2021).
7. N. Balthasar, L. T. Dalgaard, C. E. Lee, J. Yu, H. Funahashi, T. Williams, M. Ferreira, V. Tang, R. A. McGovern, C. D. Kenny, L. M. Christiansen, E. Edelstein, B. Choi, O. Boss, C. Aschkenasi, C. Y. Zhang, K. Mountjoy, T. Kishi, J. K. Elmquist, B. B. Lowell, Divergence of melanocortin pathways in the control of food intake and energy expenditure. *Cell* **123**, 493–505 (2005).
8. A. S. Garfield, C. Li, J. C. Madara, B. P. Shah, E. Webber, J. S. Steger, J. N. Campbell, O. Gavrilova, C. E. Lee, D. P. Olson, J. K. Elmquist, B. A. Tannous, M. J. Krashes, B. B. Lowell, A neural basis for melanocortin-4 receptor-regulated appetite. *Nat. Neurosci.* **18**, 863–871 (2015).
9. L. Madisen, T. A. Zwingman, S. M. Sunkin, S. W. Oh, H. A. Zariwala, H. Gu, L. L. Ng, R. D. Palmiter, M. J. Hawrylycz, A. R. Jones, E. S. Lein, H. Zeng, A robust and high-throughput Cre reporting and characterization system for the whole mouse brain. *Nat. Neurosci.* **13**, 133–140 (2010).
10. B. R. Herb, H. J. Glover, A. Bhaduri, C. Colantuoni, T. L. Bale, K. Siletti, R. Hodge, E. Lein, A. R. Kriegstein, C. A. Doege, S. A. Ament, Single-cell genomics reveals region-specific developmental trajectories underlying neuronal diversity in the human hypothalamus. *Sci. Adv.* **9**, eadf6251 (2023).
11. H. Liu, T. Kishi, A. G. Roseberry, X. Cai, C. E. Lee, J. M. Montez, J. M. Friedman, J. K. Elmquist, Transgenic mice expressing green fluorescent protein under the control of the melanocortin-4 receptor promoter. *J. Neurosci.* **23**, 7143–7154 (2003).
12. P. B. Daniel, C. Fernando, C. S. Wu, R. Marnane, R. Broadhurst, K. G. Mountjoy, 1 kb of 5′ flanking sequence from mouse MC4R gene is sufficient for tissue specific expression in a transgenic mouse. *Mol. Cell. Endocrinol.* **239**, 63–71 (2005).
13. L. M. Dumont, C. S. Wu, C. J. Aschkenasi, J. K. Elmquist, B. B. Lowell, K. G. Mountjoy, Mouse melanocortin-4 receptor gene 5′-flanking region imparts cell specific expression in vitro. *Mol. Cell. Endocrinol.* **184**, 173–185 (2001).
14. D. Acampora, M. P. Postiglione, V. Avantaggiato, M. Di Bonito, F. M. Vaccarino, J. Michaud, A. Simeone, Progressive impairment of developing neuroendocrine cell lineages in the hypothalamus of mice lacking the *Orthopedia* gene. *Genes Dev.* **13**, 2787–2800 (1999).
15. J. L. Michaud, T. Rosenquist, N. R. May, C. M. Fan, Development of neuroendocrine lineages requires the bHLH-PAS transcription factor SIM1. *Genes Dev.* **12**, 3264–3275 (1998).

Xu *et al.*, *Sci. Transl. Med.* **17**, eadr6459 (2025)   15 January 2025

10 of 11

16. J. W. Sohn, L. E. Harris, E. D. Berglund, T. Liu, L. Vong, B. B. Lowell, N. Balthasar, K. W. Williams, J. K. Elmquist, Melanocortin 4 receptors reciprocally regulate sympathetic and parasympathetic preganglionic neurons. *Cell* **152**, 612–619 (2013).

17. J. Rossi, N. Balthasar, D. Olson, M. Scott, E. Berglund, C. E. Lee, M. J. Choi, D. Lauzon, B. B. Lowell, J. K. Elmquist, Melanocortin-4 receptors expressed by cholinergic neurons regulate energy balance and glucose homeostasis. *Cell Metab.* **13**, 195–204 (2011).

18. B. Lee, J. Kim, T. An, S. Kim, E. M. Patel, J. Raber, S. K. Lee, S. Lee, J. W. Lee, Dlx1/2 and Otp coordinate the production of hypothalamic GHRH- and AgRP-neurons. *Nat. Commun.* **9**, 2026 (2018).

19. K. Inada, K. Tsujimoto, M. Yoshida, K. Nishimori, K. Miyamichi, Oxytocin signaling in the posterior hypothalamus prevents hyperphagic obesity in mice. *eLife* **11**, (2022).

20. B. M. Kublaoui, T. Gemelli, K. P. Tolson, Y. Wang, A. R. Zinn, Oxytocin deficiency mediates hyperphagic obesity of Sim1 haploinsufficient mice. *Mol. Endocrinol.* **22**, 1723–1734 (2008).

21. Z. Wu, Y. Xu, Y. Zhu, A. K. Sutton, R. Zhao, B. B. Lowell, D. P. Olson, Q. Tong, An obligate role of oxytocin neurons in diet induced energy expenditure. *PLOS ONE* **7**, e45167 (2012).

22. D. Huszar, C. A. Lynch, V. Fairchild-Huntress, J. H. Dunmore, Q. Fang, L. R. Berkemeier, W. Gu, R. A. Kesterson, B. A. Boston, R. D. Cone, F. J. Smith, L. A. Campfield, P. Burn, F. Lee, Targeted disruption of the melanocortin-4 receptor results in obesity in mice. *Cell* **88**, 131–141 (1997).

23. L. Moir, E. G. Bochukova, R. Dumbell, G. Banks, R. S. Bains, P. M. Nolan, C. Scudamore, M. Simon, K. A. Watson, J. Keogh, E. Henning, A. Hendricks, S. O'Rahilly, I. Barroso, UK10K consortium, A. E. Sullivan, D. C. Bersten, M. L. Whitelaw, S. Kirsch, E. Bentley, I. S. Farooqi, R. D. Cox, Disruption of the homeodomain transcription factor orthopedia homeobox (Otp) is associated with obesity and anxiety. *Mol. Metab.* **6**, 1419–1428 (2017).

24. K. Clement, H. Biebermann, I. S. Farooqi, L. Van der Ploeg, B. Wolters, C. Poitou, L. Puder, F. Fiedorek, G. Gottesdiener, G. Kleinau, N. Heyder, P. Scheerer, U. Blume-Peytavi, I. Jahnke, S. Sharma, J. Mokrosinski, S. Wiegand, A. Muller, K. Weiss, K. Mai, J. Spranger, A. Gruters, O. Blankenstein, H. Krude, P. Kuhnen, MC4R agonism promotes durable weight loss in patients with leptin receptor deficiency. *Nat. Med.* **24**, 551–555 (2018).

25. W. Wang, T. Lufkin, The murine Otp homeobox gene plays an essential role in the specification of neuronal cell lineages in the developing hypothalamus. *Dev. Biol.* **227**, 432–449 (2000).

26. M. J. Low, V. Otero-Corchon, A. F. Parlow, J. L. Ramirez, U. Kumar, Y. C. Patel, M. Rubinstein, Somatostatin is required for masculinization of growth hormone-regulated hepatic gene expression but not of somatic growth. *J. Clin. Invest.* **107**, 1571–1580 (2001).

27. U. D. Wankhade, D. J. Good, Melanocortin 4 receptor is a transcriptional target of nescient helix-loop-helix-2. *Mol. Cell. Endocrinol.* **341**, 39–47 (2011).

28. T. Schmid, S. Gunther, L. Mendler, T. Braun, Loss of NSCL-2 in gonadotropin releasing hormone neurons leads to reduction of pro-opiomelanocortin neurons in specific hypothalamic nuclei and causes visceral obesity. *J. Neurosci.* **33**, 10459–10470 (2013).

29. K. H. Wade, B. Y. H. Lam, A. Melvin, W. Pan, L. J. Corbin, D. A. Hughes, K. Rainbow, J. H. Chen, K. Duckett, X. Liu, J. Mokrosinski, A. Morseburg, S. Neaves, A. Williamson, C. Zhang, I. S. Farooqi, G. S. H. Yeo, N. J. Timpson, S. O'Rahilly, Loss-of-function mutations in the melanocortin 4 receptor in a UK birth cohort. *Nat. Med.* **27**, 1088–1096 (2021).

30. J. H. Bushweller, Targeting transcription factors in cancer—from undruggable to reality. *Nat. Rev. Cancer* **19**, 611–624 (2019).

31. A. E. Hendricks, E. G. Bochukova, G. Marenne, J. M. Keogh, N. Atanassova, R. Bounds, E. Wheeler, V. Mistry, E. Henning, A. Korner, D. Muddyman, S. McCarthy, A. Hinney, J. Hebebrand, R. A. Scott, C. Langenberg, N. J. Wareham, P. Surendran, J. M. Howson, A. S. Butterworth, J. Danesh, B. G. Nordestgaard, S. F. Nielsen, S. Afzal, S. Papadia, S. Ashford, S. Garg, G. L. Millhauser, R. I. Palomino, A. Kwasniewska, I. Tachmazidou, S. O'Rahilly, E. Zeggini, I. Barroso, I. S. Farooqi, Rare variant analysis of human and rodent obesity genes in individuals with severe childhood obesity. *Sci. Rep.* **7**, 4394 (2017).

32. G. Marenne, A. E. Hendricks, A. Perdikari, R. Bounds, F. Payne, J. M. Keogh, C. J. Lelliott, E. Henning, S. Pathan, S. Ashford, E. G. Bochukova, V. Mistry, A. Daly, C. Hayward, U. K. K. C. Interval, N. J. Wareham, S. O'Rahilly, C. Langenberg, E. Wheeler, E. Zeggini, I. S. Farooqi, I. Barroso, Exome sequencing identifies genes and gene sets contributing to severe childhood obesity, linking PHIP variants to repressed *POMC* transcription. *Cell Metab.* **31**, 1107–1119 e12 (2020).

33. A. Mo, E. A. Mukamel, F. P. Davis, C. Luo, G. L. Henry, S. Picard, M. A. Urich, J. R. Nery, T. J. Sejnowski, R. Lister, S. R. Eddy, J. R. Ecker, J. Nathans, Epigenomic signatures of neuronal diversity in the mammalian brain. *Neuron* **86**, 1369–1384 (2015).

34. L. A. Quina, J. Harris, H. Zeng, E. E. Turner, Specific connections of the interpeduncular subnuclei reveal distinct components of the habenulopeduncular pathway. *J. Comp. Neurol.* **525**, 2632–2656 (2017).

35. C. Liu, T. Maejima, S. C. Wyler, G. Casadesus, S. Herlitze, E. S. Deneris, Pet-1 is required across different stages of life to regulate serotonergic function. *Nat. Neurosci.* **13**, 1190–1198 (2010).

36. B. Xu, X. Tang, M. Jin, H. Zhang, L. Du, S. Yu, J. He, Unifying developmental programs for embryonic and postembryonic neurogenesis in the zebrafish retina. *Development* **147**, dev185660 (2020).

37. H. Hu, Y. R. Miao, L. H. Jia, Q. Y. Yu, Q. Zhang, A. Y. Guo, AnimalTFDB 3.0: A comprehensive resource for annotation and prediction of animal transcription factors. *Nucleic Acids Res.* **47**, D33–D38 (2019).

38. G. Yu, L. G. Wang, Y. Han, Q. Y. He, clusterProfiler: An R package for comparing biological themes among gene clusters. *OMICS* **16**, 284–287 (2012).

39. F. Yu, V. G. Sankaran, G. C. Yuan, CUT&RUNTools 2.0: A pipeline for single-cell and bulk-level CUT&RUN and CUT&Tag data analysis. *Bioinformatics* **38**, 252–254 (2021).

40. J. J. Reske, M. R. Wilson, R. L. Chandler, ATAC-seq normalization method can significantly affect differential accessibility analysis and interpretation. *Epigenet. Chromatin* **13**, Article ID 22, (2020).

41. A. T. Lun, G. K. Smyth, csaw: A Bioconductor package for differential binding analysis of ChIP-seq data using sliding windows. *Nucleic Acids Res.* **44**, e45 (2016).

42. G. Yu, L. G. Wang, Q. Y. He, ChIPseeker: An R/Bioconductor package for ChIP peak annotation, comparison and visualization. *Bioinformatics* **31**, 2382–2383 (2015).

43. L. Li, B. Xu, C. Liu, Sample enrichment for single-nucleus sequencing using concanavalin A-conjugated magnetic beads. *STAR Protoc.* **4**, 102595 (2023).